RSC Advances

PAPER

View Article Online
View Journal | View Issue

Cite this: *RSC Adv.*, 2015, **5**, 45201

Multifunctional polybenzoxazine nanocomposites containing photoresponsive azobenzene units, catalytic carboxylic acid groups, and pyrene units capable of dispersing carbon nanotubes†

Mohamed Gamal Mohamed,[a] Chi-Hui Hsiao,[a] Faliang Luo,[b] Lizong Dai[c] and Shiao-Wei Kuo*[a]

Received 1st April 2015
Accepted 14th May 2015

DOI: 10.1039/c5ra07983g

www.rsc.org/advances

In this study, we synthesized a new multifunctional benzoxazine monomer Azo-COOH-Py BZ—featuring an azobenzene unit, a carboxylic acid group, and a pyrene moiety—through the reaction of 4-(4-hydroxyphenylazo)benzoic acid (Azo-COOH), paraformaldehyde, and aminopyrene (Py-NH_2) in 1,4-dioxane. Fourier transform infrared (FTIR) spectroscopy and ^1H and ^{13}C nuclear magnetic resonance spectroscopy confirmed the structure of this new monomer. Using differential scanning calorimetry (DSC), thermogravimetric analysis (TGA), and FTIR spectroscopy, we monitored the curing behavior of Azo-COOH-Py BZ leading to the formation of poly(Azo-COOH-Py BZ); we found that the carboxylic acid and azobenzene units acted as catalysts for the ring opening reaction of the benzoxazine unit. The pyrene moiety of Azo-COOH-Py BZ enhanced the dispersibility of carbon nanotubes (CNTs) in THF, leading to the formation of highly dispersible Azo-COOH-Py BZ/CNT nanocomposites stabilized through $\pi-\pi$ stacking of the pyrene and CNT units, as detected through fluorescence emission spectroscopy. We also used DSC and TGA to examine the curing behavior of Azo-COOH-Py BZ/CNTs to form poly(Azopy-COOH-Py BZ)/CNTs nanocomposites. Interestingly, DSC profiles revealed that the maximum exothermic peak representing the ring opening polymerization of the benzoxazine unit of Azo-COOH-Py BZ shifted to much lower temperature upon increasing the content of single-walled CNTs (SWCNTs) or multiwalled CNTs (MWCNTs), suggesting that the CNTs acted as catalysts for the ring opening reaction of the benzoxazine. In addition, the curing temperatures for the SWCNT composites were lower than those for the MWCNT composites, suggesting that the SWCNTs were dispersed better than the MWCNTs in their composites and that the thermal stability of the SWCNT nanocomposites was higher than that of the MWCNT nanocomposites. The combination of photoresponsive azobenzene units, carboxylic acid groups, and CNTs enhanced the thermal stability and char yields of the polybenzoxazine matrixes, as determined through TGA analyses.

Introduction

Polybenzoxazines (PBZs) are recently developed thermosetting phenolic resins that are attracting academic and industrial interest because they possess several unique properties, including low degrees of water absorption, near-zero volumetric shrinkage, low surface free energies, high glass transition temperatures, excellent resistance toward chemicals and excellent physical and mechanical properties relative to those of other thermosetting resins.[1–4] In addition, low dielectric constants and low flammability make them attractive materials for use in many applications.[3–11] PBZs can be obtained through polymerization, *via* heterocyclic ring opening, of corresponding benzoxazine (BZ) monomers at elevated temperature, without the need for strong acids or bases and without releasing byproducts.[12–14]

Although they are promising materials, it remains necessary to improve the performance of PBZs. The mechanical properties of PBZs can be enhanced through the addition of inorganic materials, including glass fibers,[15] carbon fibers,[16] polyhedral oligomeric silsesquioxane (POSS),[17–20] graphene

[a]*Department of Materials and Optoelectronic Science, Center for Functional Polymers and Supramolecular Materials, National Sun Yat-Sen University, Kaohsiung, Taiwan. E-mail: kuosw@faculty.nsysu.edu.tw*

[b]*Key Laboratory of Energy Resources & Chemical Engineering, Ningxia University, Ministry-Province Co-cultivated State Key Laboratory Base of Natural Gas Conversion, Yinchuan 750021, China*

[c]*Department of Material Science and Engineering, Fujian Provincial Key Laboratory of Fire Retardant Materials, College of Materials, Xiamen University, Xiamen, Fujian, 361005, China*

† Electronic supplementary information (ESI) available: DSC analyses of the thermal curing behavior of Py-BZ, Azo-COOH, Azo-COOH-Py BZ, and the Azo-COOH-Py BZ/MWCNT complex. See DOI: 10.1039/c5ra07983g

oxide,[21] and carbon nanotubes (CNTs).[22–30] CNTs are hexagonal arrays of rolled carbon sheets having lengths of several microns and diameters of a few nanometers. Based on the number of carbon layers in the wall, these structures can be classified into either single-walled carbon nanotubes (SWCNTs) or multiwalled carbon nanotubes (MWCNTs).[31,32] CNTs are materials of interest for academic research and industrial applications because they possess many unique chemical and physical properties,[33,34] including high stiffness, strength, and thermal conductivity arising from the graphitic nature of the nanotube lattice.[22] Two general approaches have been reported to increase the miscibility of CNTs in PBZ matrices: covalent functionalization and noncovalent adsorption of organic molecules onto CNT surfaces. The first approach involves covalently bonding surface-modifying groups or molecules onto the CNTs to enhance their dispersion in solvents and/or polymer matrices.[23,24] For example, PBZ-modified MWCNTs have been prepared after sequential treatment of MWCNTs with HNO_3 and toluene-2,4-diisocyanate to introduce OH, COOH, and N=C=O groups, with the surface COOH groups then catalyzing the opening of benzoxazine rings.[22,25] In addition, Chen *et al.* reported that the surface carboxyl groups of CNTs catalyze the ring opening process and decrease the curing temperature of BZ monomers.[22] Nevertheless, the covalent functionalization of MWCNTs will destroy their optical, electronic, and mechanical properties, because of the inevitable change in orbital hybridization of some of their carbon atoms from sp^2 to sp^3.[26] The second approach, involving noncovalent interactions between organic PBZs and CNTs, generally preserves nearly all of the intrinsic features of the CNTs. Dumas *et al.* reported that π-stacking interactions between CNTs and a phenylenediamine-based BZ led to the formation of a reinforced network displaying excellent thermal and mechanical properties, with enhanced dispersion of the unreacted MWCNTs in the PBZ matrix.[27] Wang *et al.* reported a BZ derivative that behaved as an attractive noncovalent dispersant for CNTs, leading to functionalized CNTs exhibiting high dispersibility in an organic solvent.[26] In addition, we have developed a pyrene-based BZ precursor that forms PBZ/CNT nanocomposites stabilized through strong π–π interactions between the pyrene units and CNT surfaces.[28,29] We found, however, that the model pyrene-functionalized BZ (Py-BZ) prepared from phenol, formaldehyde, and 1-aminopyrene exhibited a relatively high exothermic ring opening temperature of 286.0 °C.[28]

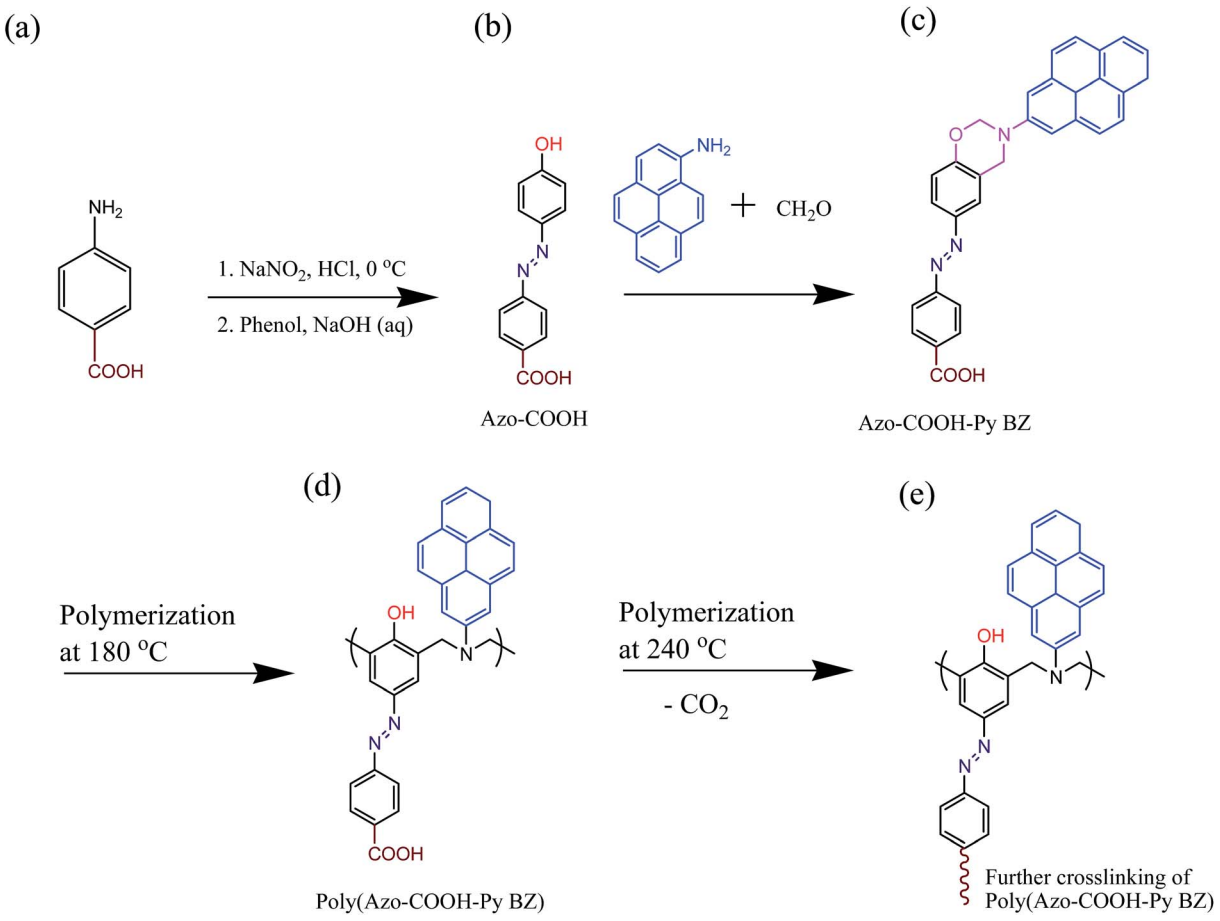

Scheme 1 (a) 4-Aminobenzoic acid and synthesis of (b) Azo-COOH, (c) Azo-COOH-Py BZ, (d) poly(Azo-COOH-Py BZ) and (e) further crosslinking of poly(Azo-COOH-Py BZ).

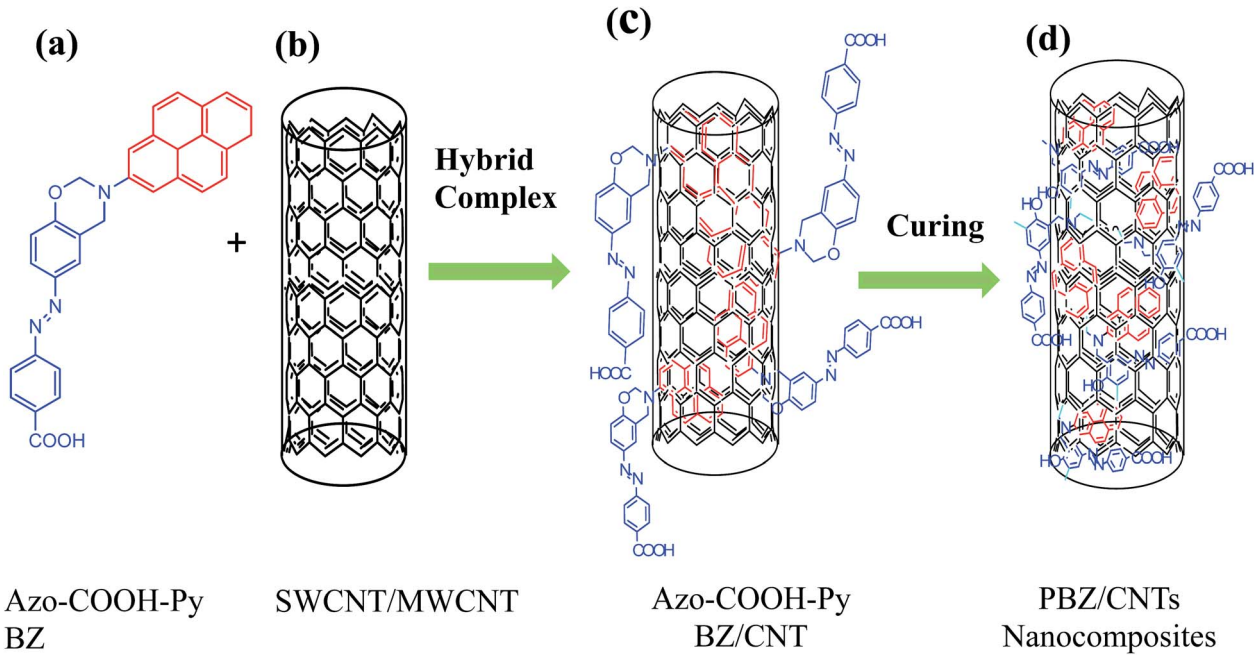

Scheme 2 The possible Azo-COOH-Py BZ/CNT hybrid complex and after thermal curing to form PBZ/CNTs nanocomposites.

PBZs are also interesting materials because strong intramolecular hydrogen bonding interactions remain after curing and because of their extremely low surface energies—in some cases lower than that of pure Teflon.[4] Nevertheless, the need for high curing temperatures can limit the applications of PBZs, especially as polymer coatings.[5,9] In a previous study, we found that Azo-COOH BZ, a monomer containing both azobenzene and COOH units, exhibits polymerization temperature much lower than that of traditional BZ monomers.[35] Polymers containing azobenzene moieties are interesting because of their ability to undergo reversible photoisomerization or thermal *cis*-to-*trans* isomerization processes. Thus, the incorporation of azobenzene moieties into PBZs can impart them with thermally regulated behavior after being subjected to changes in the amount of incident light or heat.[36–38] Indeed, Kiskan *et al.* synthesized an azobenzene functionalized BZ that exhibited high thermal stability arising from the presence of the additional aromatic group.[39]

As a result, we wished to examine the combination of a photoresponsive azobenzene unit, a catalytic COOH group, and a pyrene unit (for dispersing CNTs) within a BZ monomer, allowing the formation of high-performance PBZ/CNT nanocomposites. Without the need to functionalize CNTs with COOH groups, PBZ/CNT nanocomposites derived from such a multifunctional BZ monomer, which can itself catalyze the opening of the BZ ring (through its COOH units), would feature high dispersion of the CNTs in the polymer matrix, stabilized through π–π interactions between the pyrene units and the CNT surfaces, thereby overcoming the problems associated with covalently functionalized CNTs while retaining the photoresponsive azobenzene units to mediate changes in the surface properties upon the application of light and/or heat. Thus, in this study we prepared Azo-COOH-Py BZ through the reaction of Azo-COOH, paraformaldehyde, and 1-aminopyrene in 1,4-dioxane [Scheme 1] and then used it to form poly(Azo-COOH-Py)/CNT nanocomposites with SWCNTs and MWCNTs [Scheme 2]. Differential scanning calorimetry (DSC), Fourier transform infrared (FTIR) spectroscopy, and thermogravimetric analysis (TGA) revealed the thermal curing behavior and thermal stability of the BZ monomer, both before and after blending with various weight percentages of SWCNTs and MWCNTs. In addition, we used photoluminescence spectroscopy and transmission electron microscopy (TEM) to investigate the interactions and dispersions of the SWCNTs and MWCNTs with the PBZ matrices before and after thermal curing.

Experimental section

Materials

Paraformaldehyde (96%), pyrene, NaOH, Na_2CO_3, 4-aminobenzoic acid, $CHCl_3$, CH_2Cl_2, EtOH, tetrahydrofuran (THF), and 1,4-dioxane were purchased from Acros. Ethyl acetoacetate was purchased from Showa. HNO_3 (65%), AcOH (99.8%), and H_2SO_4 (65%) were purchased from Scharlau. Hydrazine monohydrate (98%) was purchased from Alfa Aesar. 1-Nitropyrene was synthesized using a previously reported procedure.[28] SWCNTs and MWCNTs were purchased from Center Biochemistry Technology.

Pyren-1-amine (Py-NH_2)

In a modified version of a procedure reported our literature,[28] 1-nitropyrene (10.0 g, 40.5 mmol) and 10% Pd/C (0.2 g) were dissolved/suspended in absolute EtOH (250 mL) and THF (150 mL) under N_2 in a 500 mL two-neck round-bottom flask equipped with a stirrer bar. The suspension was heated under reflux at 90 °C and then hydrazine monohydrate (15 mL) was

added dropwise. After heating under reflux for a further 24 h, the mixture was cooled and filtered; the filtrate was evaporated to dryness under reduced pressure. The crude product was recrystallized from cyclohexane and then further purified through column chromatography (*n*-hexane/THF, 3 : 1). Drying at 40 °C gave greenish yellow crystals (7.50 g, 85%); m.p.: 115–117 °C (DSC). FTIR (KBr, cm^{-1}): 3200–3400 (NH stretch). ^1H NMR (500 MHz, DMSO-d_6, δ, ppm): 6.34 (s, 2H, NH_2), 7.34–8.28 (m, 9H, CCH). ^{13}C NMR (125 MHz, DMSO-d_6, δ, ppm): 113.0 ($CHCHNH_2$), 121.1–132.9 (aromatic), 144.4 ($CHNH_2$).

4-(4-Hydroxphenyazo)benzoic acid (Azo-COOH)

In a modified version of a procedure reported in the literature,[35] a solution of 4-aminobenzoic acid (13.7 g, 0.100 mol) in dilute HCl [a mixture of conc. HCl (20 mL) in water (20 mL)] was diazotized through the addition of a solution of sodium nitrite (6.90 g, 0.1 mol) in water (20 mL). The mixture was stirred at 0 °C and then diluted with cold MeOH (300 mL). Phenol (9.41 g, 0.100 mol), dissolved in a cooled solution of NaOH (10.8 g, 0.190 mol) in MeOH (50 mL), was added dropwise to the solution containing the diazonium salt. A red dye formed; this mixture was stirred for 2 h and then poured into dilute HCl (0.5 N) with stirring for 1 h. The red solid was filtered off, washed many times with deionized water, dried, and recrystallization ($MeOH/H_2O$, 1 : 1) to give the product (9.00 g, 66%); m.p.: 273–275 °C (DSC). FTIR (KBr, cm^{-1}): 3463–3204 (OH stretch), 3053–2500 (COOH), 1660 (C=O stretch). ^1H NMR (500 MHz, DMSO-d_6, δ, ppm): 6.88–8.12 (m, 8H, ArH), 10.17 (s, 1H, OH), 13.13 (s, 1H, COOH). ^{13}C NMR (125 MHz, DMSO-d_6, δ, ppm): 167.20 (C=O).

(*E*)-4-[3-(Pyren-2-yl)-3,4-dihydro-2*H*-benzoxazin-6-yl] diazenylbenzoic acid (Azo-COOH-Py BZ)

A solution of 1-aminopyrene (1.00 g, 4.60 mmol) in 1,4-dioxane (25 mL) was added portionwise to a stirred solution of paraformaldehyde (0.290 g, 9.67 mmol) in 1,4-dioxane (50 mL) in a 150 mL three-neck round-bottom flask cooled in an ice bath. The mixture was then stirred for 30 min while maintaining the temperature below 5 °C. A solution of 4-(4-hydroxphenyazo)benzoic acid (0.810 g, 5.06 mmol) in 1,4-dioxane (30 mL) was added; the mixture was degassed three times and then heated under reflux for 24 h at 80–90 °C while stirring. After cooling the mixture to room temperature, the solvent was evaporated under reduced pressure to give a yellow solid, which was extracted into Et_2O (3 × 80 mL); the combined extracts were washed several times with 5% Na_2CO_3 and finally with distilled water. The organic phase was dried (anhydrous $MgSO_4$) for 1 h and then concentrated under reduced pressure to afford a yellow solid, which was purified through column chromatography (SiO_2; *n*-hexane/EA, 1 : 1) to give a yellow solid (0.94 g, 73%). FTIR (KBr, cm^{-1}): 3053–2500 (COOH), 1232 (asymmetric COC stretching), 1341 (CH_2 wagging), 931 and 1490 (vibration of trisubstituted benzene ring), 1660 (C=O stretching). ^1H NMR (500 MHz, DMSO-d_6, δ, ppm): 4.84 (s, 2H, $ArCH_2N$), 5.59 (s, 2H, OCH_2N), 6.92–8.43 (m, ArH). ^{13}C NMR (125 MHz, DMSO-d_6, δ, ppm): 48.47 ($ArCH_2N$), 80.04 (OCH_2N), 113.7–157.8 (aromatic), 160.5 (C=O).

Photoisomerization of Azo-COOH-Py BZ

A solution of Azo-COOH-Py BZ (1×10^{-4} M) in THF (10 mL) was placed in a quartz tube and irradiated for intervals of time at room temperature in a merry-go-round-type photoreactor equipped with five Philips lamps emitting light nominally at 365 nm.

Poly(Azopy-COOH BZ) films

A solution of Azo-COOH-Py BZ monomer (4 wt%) in THF was passed through a 0.3 μm syringe filter and then a portion (1 mL) was spin-coated (1500 rpm, 50 s) onto a glass slide (1000 mm × 100 mm × 1 mm). After thermal curing, the poly(Azo-COOH-Py BZ) films were examined for their surface behavior.

Azo-COOH-Py BZ/CNT nanocomposites

CNTs (SWCNTs or MWCNTs) were first dispersed at various weight percentages in THF, under ultrasonic vibration for 2 h. Each of the resulting solutions was mixed with the Azo-COOH-Py BZ monomer. The solvent was evaporated in a vacuum oven at 50 °C for 1 day. The blend mixtures were then poured into a stainless-steel mold and subjected to thermal curing in a stepwise manner (heating at 110, 150, 180, 210, and 240 °C, for 2 h at each temperature). The color of each sample was dark-red.

Characterization

^1H and ^{13}C nuclear magnetic resonance (NMR) spectra were recorded using an INOVA 500 instrument with DMSO-d_6 and $CDCl_3$ as solvents and tetramethylsilane (TMS) as the external standard. FTIR spectra of the BZ monomer and PBZ polymer were recorded using a Bruker Tensor 27 FTIR spectrophotometer and the conventional KBr disk method; 32 scans were collected at a spectral resolution of 4 cm^{-1}. The films tested in this study were sufficiently thin to obey the Beer–Lambert law. FTIR spectra recorded at elevated temperatures were obtained from a cell mounted inside the temperature-controlled compartment of the spectrometer. Dynamic curing kinetics were determined using a TA Q-20 differential scanning calorimeter operated under a N_2 atmosphere. The sample (*ca.* 5 mg) was placed in a sealed aluminum sample pan. Dynamic curing scans were recorded from 30 to 350 °C at a heating rate of 20 °C min^{-1}. The thermal stabilities of the samples were measured using a TA Q-50 thermogravimetric analyzer operated under a N_2 atmosphere. A cured sample (*ca.* 5 mg) was placed in a Pt cell and heated at a rate of 20 °C min^{-1} from 30 to 800 °C under a N_2 flow rate of 60 mL min^{-1}. UV-Vis spectra were recorded using a Shimadzu mini 1240 spectrophotometer; the concentration of Azo-CCOH-Py BZ in THF was 10^{-4} M. Photoisomerization of azobenzene moieties was performed directly under a UV-Vis lamp at 365 nm (90 mW cm^{-1}). Photoluminescence (PL) excitation and emission spectra were recorded at room temperature using a monochromatized Xe light source. TEM images were recorded using a JEOL-2100 transmission electron microscope operated at an accelerating voltage of 200 kV.

Results and discussion

Synthesis of Azo-COOH-Py BZ monomer

^{1}H NMR, ^{13}C NMR and FT-IR spectroscopy confirmed the chemical structure of the Azo-COOH-Py BZ monomer, which we synthesized in high yield through Mannich condensation of Azo-COOH, 1-aminopyrene, and paraformaldehyde in 1,4-dioxane at 90 °C (Scheme 1). Fig. 1 displays the ^{1}H NMR spectra of Azo-COOH, 1-aminopyrene, and Azo-COOH-Py BZ. The spectrum of Azo-COOH [Fig. 1(a)] features signals at 10.47 and 13.13 ppm representing the OH groups of the phenolic and COOH units, respectively; the signals of the aromatic protons of Azo-COOH appeared in the range 6.97–8.10 ppm. The spectrum of Py-NH_2 [Fig. 1(b)] features a characteristic peak at 6.33 ppm for the NH proton. The ^{1}H NMR spectrum of Azo-COOH-Py BZ monomer [Fig. 1(c)] displays characteristic signals for the oxazine ring protons of Azo-COOH-Py BZ as two singlets at 4.9 and 5.7 ppm, which we assign to the $ArCH_2N$ and OCH_2N units, respectively; the signals of the NH proton of Py-NH_2 and the OH proton of Azo-COOH were absent, but the signal for the COOH group remained along with multiple signals at 6.5–8.4 ppm representing aromatic protons. Fig. 2 presents the ^{13}C NMR spectra of Azo-COOH, Py-NH_2, and Azo-COOH-Py BZ. In the spectrum of Azo-COOH [Fig. 2(a)], the signals of the azobenzene moiety appear in the range 116.6–162.3 ppm, with a signal at 167.2 ppm representing to C=O group. The spectrum of Py-NH_2 features signals for the pyrenyl aromatic ring in the range 113.1–144.4 ppm [Fig. 2(b)]. The spectrum of Azo-COOH-Py BZ [Fig. 2(c)] reveals characteristic signals for the carbon nuclei of the oxazine ring at 51.9 and 82.9 ppm ($ArCH_2N$ and OCH_2N, respectively) and a signal at 167.5 ppm for the C=O group. Fig. 3 presents the FTIR spectra recorded at ambient temperature of Azo-COOH, Py-NH_2, Azo-COOH-Py BZ, and, after thermal curing, poly(Azo-COOH-Py BZ). The spectrum of Azo-COOH [Fig. 3(a)] features a broad signal at 3053–2523 cm^{-1} for the hydrogen-bonded COOH dimer and sharp signals at 3470 and 3540 cm^{-1} corresponding to the hydrogen-bonded and free OH groups, respectively. The spectrum of Py-NH_2 [Fig. 3(b)] contains a sharp signal for the amino group at 3200–3460 cm^{-1}, with absorption bands of the pyrene unit at 831, 1599, 1619, and 3033 cm^{-1}. The FTIR spectrum of Azo-COOH-Py BZ monomer [Fig. 3(c)] displays characteristic absorption bands at 1228 (asymmetric COC stretching), 1073 (symmetric COC stretching), and 920 (stretching vibrations of oxazine ring) cm^{-1}, as well as a band at 1376 cm^{-1} representing the tetrasubstituted benzene ring and a band at 1670 cm^{-1} representing the C=O group. Fig. 3(d) presents FTIR spectra of the pure Azo-COOH-Py BZ monomer recorded after each thermal curing cycle. The characteristic absorption bands of the trisubstituted aromatic ring of Azo-COOH-Py BZ (1490 and 920 cm^{-1}) disappeared after thermal curing, while broad absorption bands, representing different types of hydrogen bonding interactions, appeared at 2500–3500 cm^{-1}. All this information from the ^{1}H, ^{13}C NMR, and FTIR spectra is consistent with the successful synthesis of the Azo-COOH-Py BZ monomer.

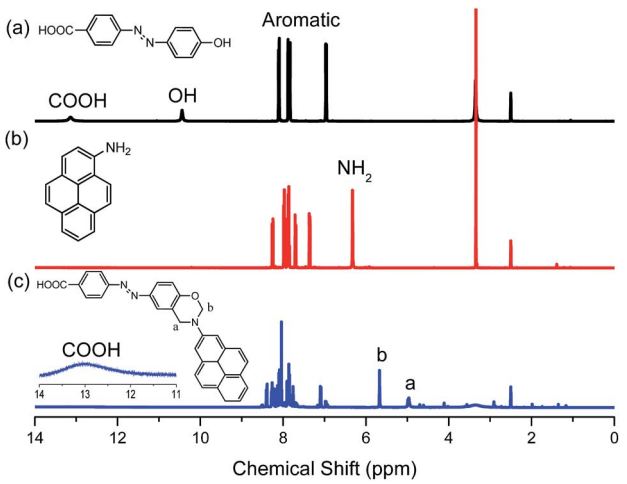

Fig. 1 ^{1}H NMR spectra of (a) Azo-COOH, (b) Py-NH_2, and (c) Azo-COOH-Py BZ.

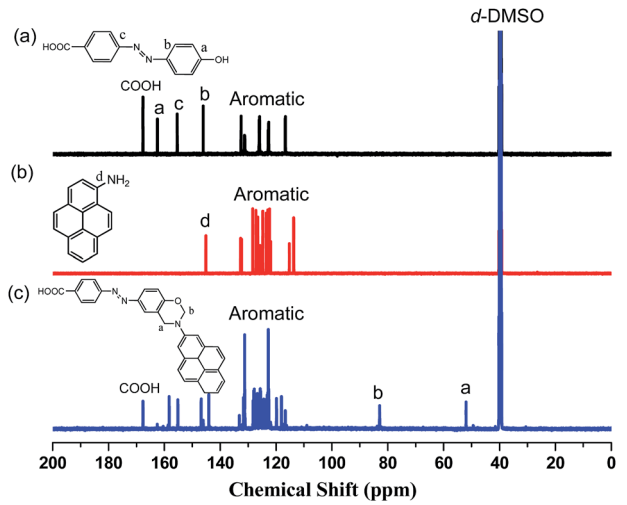

Fig. 2 ^{13}C NMR spectra of (a) Azo-COOH, (b) Py-NH_2, and (c) Azo-COOH-Py BZ.

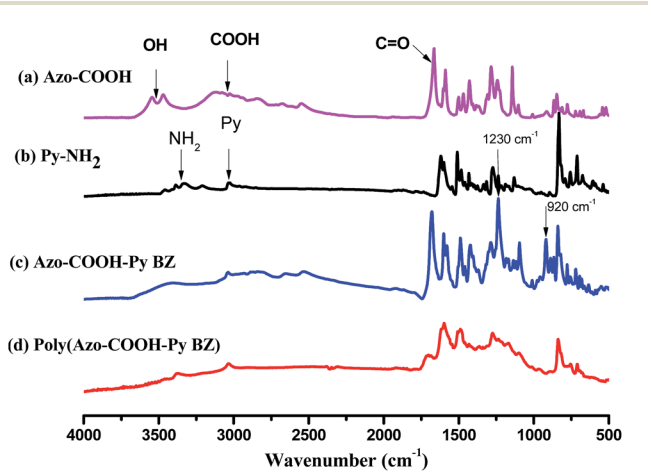

Fig. 3 FTIR spectra of (a) Azo-COOH, (b) Py-NH_2, (c) Azo-COOH-Py BZ, and (d) poly(Azo-COOH-Py BZ), recorded at room temperature.

Thermal curing behavior of Azo-COOH-Py BZ monomer

To better understand the ring opening polymerization and thermal curing behavior of the Azo-COOH-Py BZ monomer, we used DSC to investigate the thermal polymerization and curing temperature of the Azo-COOH-Py BZ monomer and FTIR spectroscopy to monitor changes in the absorption signal of the BZ ring. Fig. 4(A) presents DSC thermograms of Azo-COOH-Py BZ after each curing cycle, recorded at a heating rate of 20 °C min^{-1}. The DSC curves of the uncured Azo-COOH-Py BZ reveal a maximum with an exothermic peak at 226.0 °C, and a reaction heat of 324.7 J g^{-1}. This curing temperature is much lower than that of a model pyrene-functionalized BZ (Py-BZ) lacking the Azo-COOH unit;[28] its exothermic ring opening at 286.0 °C, as displayed in Fig. S1(a),† suggests that the Azo-COOH unit in Azo-COOH-Py BZ acted as a catalyst that contributed to the lower polymerization temperature. The acidic character of this reactive monomer increased the concentration of oxonium species, thereby catalyzing the ring opening reaction of the BZ unit. Nevertheless, this curing temperature is higher than that (sharp exothermic ring opening peak at 199 °C) of the uncured Azo-COOH BZ lacking the pyrene unit [Fig. S1(c)†], indicating that the bulky pyrene unit hindered the ring opening polymerization of the BZ unit. We observed two major curing peaks each for the Azo-COOH BZ and Azo-COOH-Py BZ monomers, but a single peak for the Py-BZ monomer, indicating that the Azo-COOH unit introduces another mode of curing for the BZ monomer. We believe the first exotherm arises from opening of the oxazine ring, while the second represents decarboxylation. The maximum curing temperature and the enthalpy of the

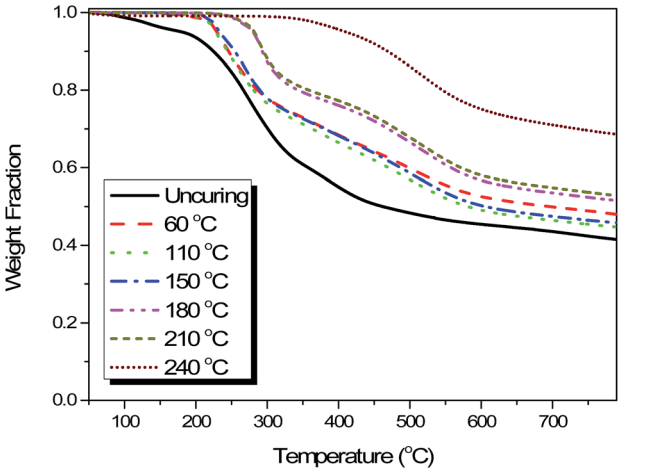

Fig. 5 TGA analyses of Azo-COOH-Py BZ, recorded after each curing stage.

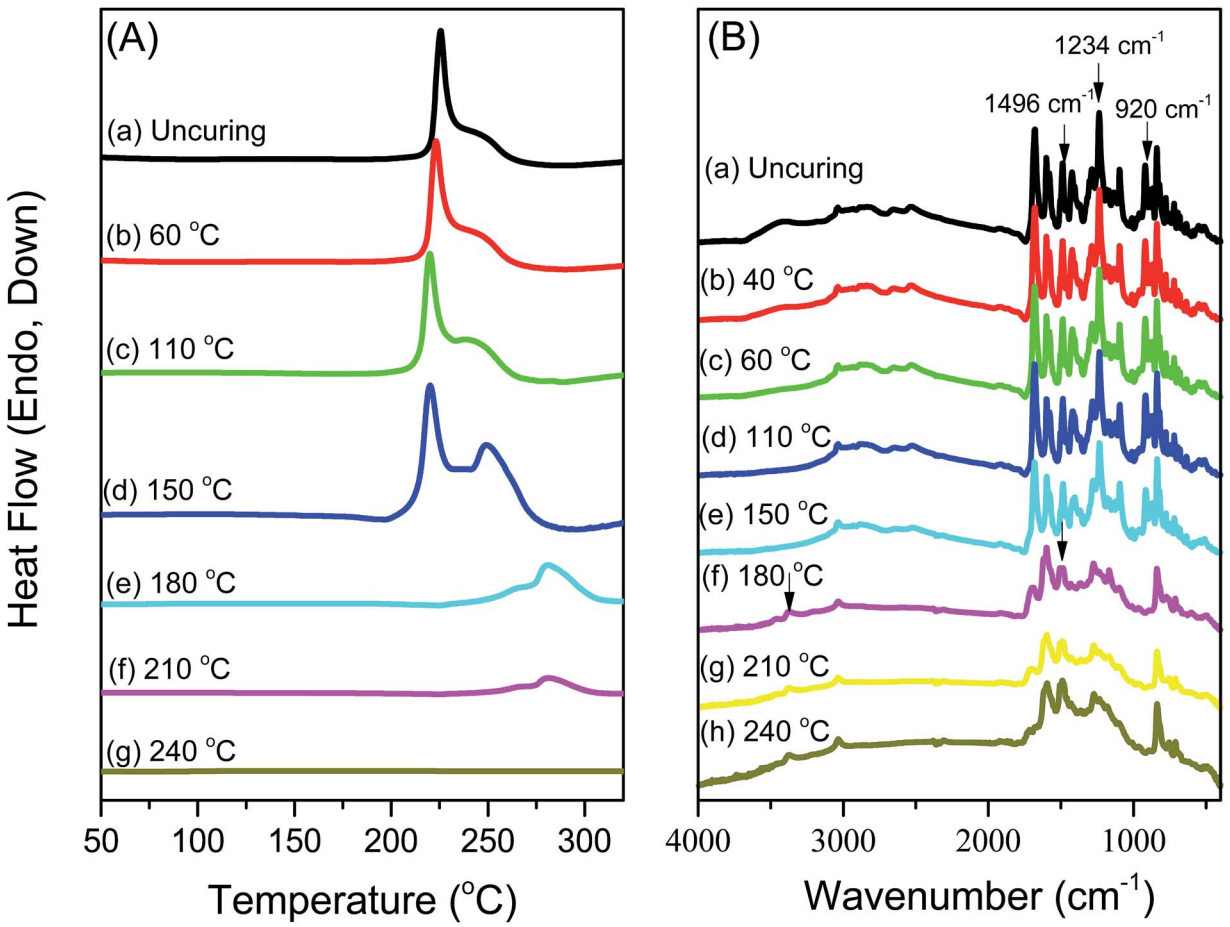

Fig. 4 (A) DSC thermograms and (B) FTIR spectra of Azo-COOH-Py BZ, recorded after each heating stage.

exotherms generally decreased upon increasing the curing temperature of Azo-COOH-Py BZ. The first exotherm, corresponding to opening of the oxazine ring, disappeared when the curing temperature was 180 °C; the second exotherm shifted to 281 °C when the curing temperature was 180 or 210 °C; and all exotherm peaks disappeared completely after applying a curing temperature of only 240 °C, indicating that thermal curing of Azo-COOH-Py BZ was complete at this temperature.

Fig. 4(B) displays FTIR spectra of the Azo-COOH-Py BZ monomer and its products after each curing stage. The intensities of the characteristic absorption bands at 1496 (stretching of trisubstituted benzene ring), 1234 (asymmetric COC stretching of oxazine), and 920 (stretching vibrations of oxazine ring) cm^{-1} decreased gradually upon increasing the curing temperature. The peak at 920 cm^{-1} disappeared completely and a new absorption appeared at 3371 cm^{-1}, corresponding to [O–H···O] intermolecular hydrogen bonding of OH groups, after opening of the oxazine ring when the curing temperature was 180 °C, consistent with the findings from our DSC analyses in which the first exotherm peak from the ring opening polymerization of the oxazine disappeared completely at 180 °C. Upon further increasing the curing temperature, the main feature in these spectra was the decreased intensity of the band corresponding to the COOH group at 1677 cm^{-1}, almost disappearing at 240 °C, indicating that thermal polymerization of this monomer proceeds with partial decarboxylation,[40] with one peak appearing at 1487 cm^{-1}, attributable to the tetrasubstituted benzene ring, that increased in intensity during the curing cycle to produce PBZ.

Fig. 5 displays the thermal stability of the Azo-COOH-Py BZ monomer after each curing stage, as determined through TGA analysis. We observe that the initial thermal decomposition temperature (T_{d5}) and char yield both increased upon increasing the curing temperature. In addition, the initial thermal decomposition temperature in Fig. 5 of each curing stage was strongly correlated with the first curing exothermic peak in the DSC traces in Fig. 4(A). For example, the value of T_{d5} increased significantly to 280 °C (similar to the exothermic peak at 281 °C determined through DSC) when the curing temperature was 180 °C, compared with a value of 230 °C when the curing temperature was 150 °C. This behavior was due to the crosslinking structure that formed [Scheme 1(d)] after thermal curing at 180 °C. Further increasing the curing temperature to 240 °C caused the value of T_{d5} to increase significantly to 396 °C, indicating a more highly cross-linked structure [Scheme 1(e)], presumably because of hydrogen bonding between the COOH groups and/or interactions involving the new reactive positions produced after decarboxylation.[40]

Photoisomerization of azobenzene chromophore in Azo-COOH-Py BZ monomer

Azobenzene moieties are well known for their reversible *trans*-to-*cis* photoisomerization upon irradiation with light.[41,42] Correspondingly, both the molecular morphology and the

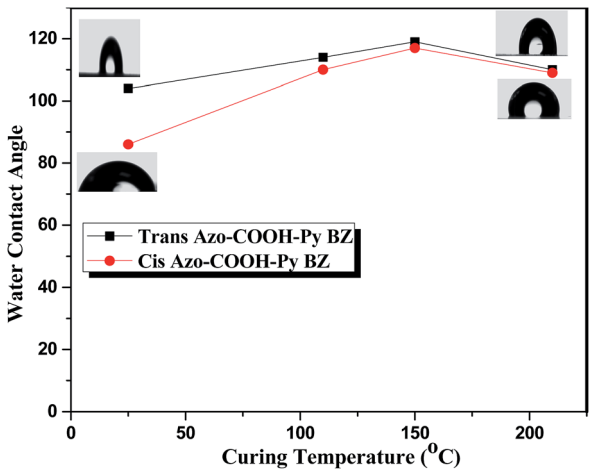

Fig. 7 WCAs of Azo-COOH-Py BZ in its *trans* and *cis* isomeric forms, recorded after each curing stage.

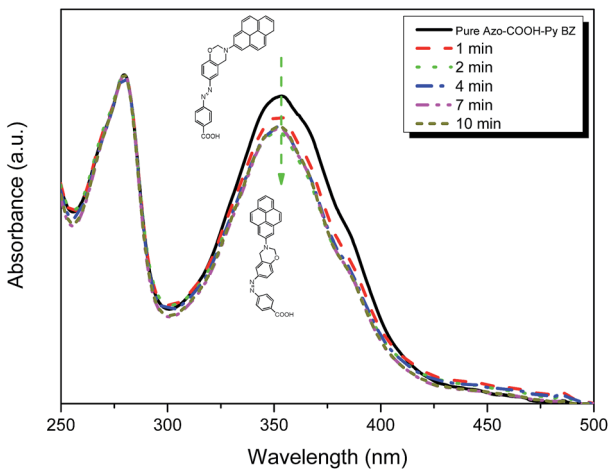

Fig. 6 Changes in UV-Vis absorbance of Azo-COOH-Py BZ in THF after irradiation at 365 nm.

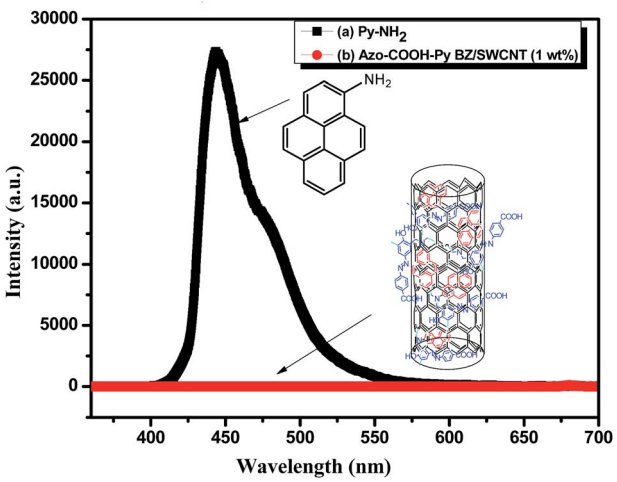

Fig. 8 PL spectra of (a) Py-NH_2 and (b) the Azo-COOH-Py BZ/SWCNT (1 wt%) hybrid complex.

dipole moment transition are greatly modified through this photochemical reaction. In the UV-Vis absorption spectra (Fig. 6), the maximum absorption wavelength decreased after photoirradiation. We monitored the photoisomerization process by measuring the change in absorption of the *trans* azobenzene unit at 352 nm, corresponding to its π–π* transition. Upon irradiation with UV light, the intensity of the absorbance at 352 nm decreased gradually, eventually reaching a relatively stable value; the signal for the *cis* isomer would increase accordingly, as expected. Fig. 7 displays the water contact angles (WCAs) for pure Azo-COOH-Py BZ before and after its photoisomerization under a UV lamp at 365 nm, as well as after thermal curing at 110, 150, and 210 °C for 2 h. The WCA of the *trans* isomer of Azo-COOH-Py BZ was larger than that of the *cis* isomer of Azo-COOH-Py BZ for all curing temperatures; this behavior is consistent with the *trans* isomer having a smaller dipole moment and lower surface free energy (and, therefore, a higher WCA) and the *cis* form possessing a bigger dipole moment and higher surface free energy (and, therefore, a lower WCA).[43] The WCAs increased upon increasing the thermal curing temperature up to 150 °C, probably because of a drying effect. After thermal curing of the Azo-COOH-Py BZ monomer at 210 °C, the WCA remained higher than that of the uncured Azo-COOH-Py BZ monomer, consistent with the network structure that formed (*cf.* DSC and FTIR analyses in Fig. 4) and the presence of different kinds of hydrogen bonding interactions. Most importantly, the degree of intramolecular [O–H···N] hydrogen bonding would increase the WCA and decrease the surface free energy relative to that for the uncured BZ monomer.[4] Nevertheless, a new absorption was evident at 3371 cm^{-1} [Fig. 4(B)], corresponding to intermolecular [O–H···O] hydrogen bonding, after opening of the oxazine ring when the curing temperature was 210 °C.[3,4] Although such intermolecular

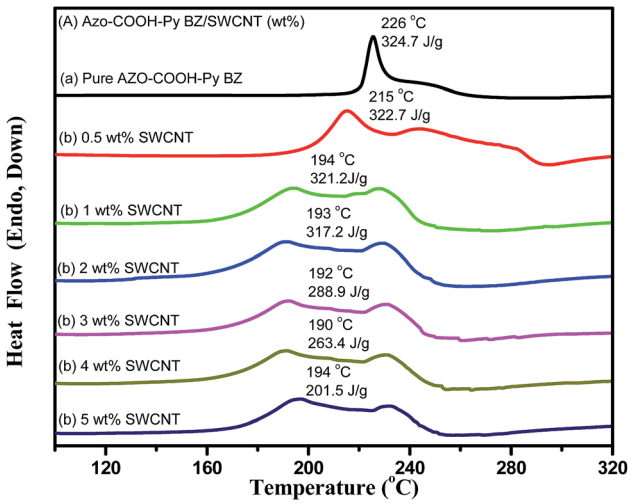

Fig. 10 DSC thermograms of the curing behavior of Azo-COOH-Py BZ/SWCNT hybrid complexes at various SWCNT contents.

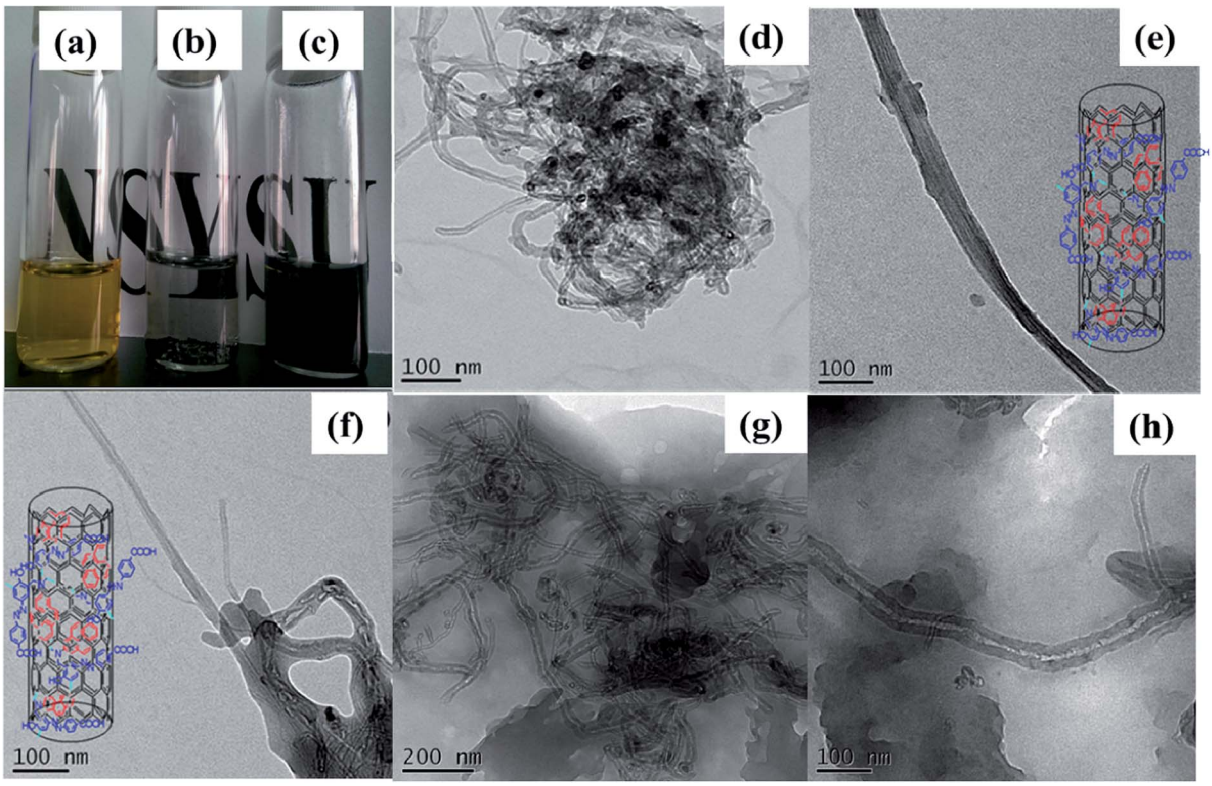

Fig. 9 (a–c) Photographs of (a) Azo-COOH-Py BZ, (b) pristine SWCNTs, and (c) Azo-COOH-Py BZ/SWCNTs (5 wt%) in THF. (d–h) TEM images of (d) pure SWCNTs, (e and f) Azo-COOH-Py BZ/SWCNTs (5 wt%) (e) before and (f) after thermal curing, and (g and h) Azo-COOH-Py BZ/MWCNTs (5 wt%) (g) before and (h) after thermal curing.

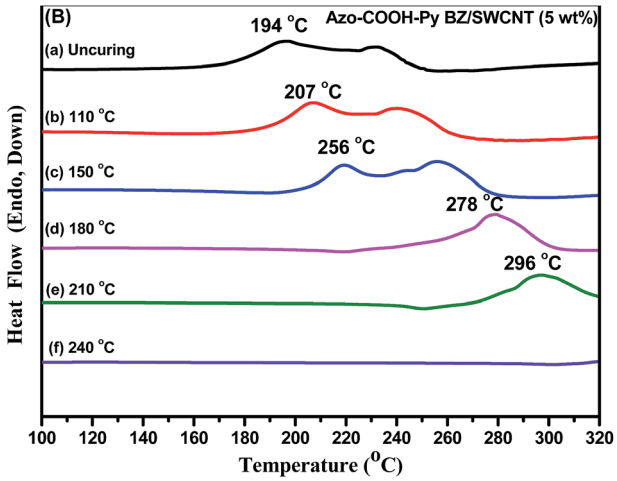

Fig. 11 DSC thermograms of the curing behavior of the Azo-COOH-Py BZ/SWCNT (5 wt%) hybrid complex after each curing stage.

[O–H···O] hydrogen bonding would decrease the WCA,[4] we also found that the WCA of the *trans* isomer remained larger than that of the *cis* isomer after each thermal curing.

Poly(Azo-COOH-Py BZ)/CNTs nanocomposites

Fig. 8 displays the fluorescence spectra of Py-BZ and the Azo-COOH-Py BZ/SWCNT complex in solution after excitation at 343 nm. The spectrum of Py-NH_2 features a strong fluorescence signal for the pyrene unit at 426 nm, while the spectrum of the Azo-COOH-Py BZ/SWCNT (1 wt%) complex features completely quenched fluorescence of the pyrene unit, indicating that strong π–π stacking existed between the pyrene moieties of the Azo-COOH-Py BZ monomers and the SWCNTs.[44] Fig. 9(a–c) display photographs of THF solutions of pure Azo-COOH-Py BZ, pure SWCNTs, and the Azo-COOH-Py BZ/SWCNT complex, respectively. Pure Azo-COOH-Py formed a clear solution, whereas the pure SWCNTs precipitated completely with strong aggregation, as confirmed in the TEM image in Fig. 9(d). In contrast, the addition of Azopy-COOH-Py BZ into the suspension of the SWCNTs resulted in a clear black solution [Fig. 9(c)], suggesting that stable complexes formed as a result of non-covalent π–π stacking. Fig. 9(e) and (f) reveal the uniform dispersions of the SWCNTs within the Az-COOH-Py BZ matrix before and after thermal curing, respectively. Similar behavior appeared for the Az-COOH-Py BZ/MWCNT nanocomposites, with Fig. 9(g) and (h) revealing the uniform dispersions of the MWCNTs within the Az-COOH-Py BZ matrix before and after thermal curing, respectively. Scheme 2 presents a possible morphology for the Az-COOH-Py BZ/CNT hybrid complexes.

We used DSC to monitor the curing behavior of the Azo-COOH-Py BZ monomer in the presence of various weight percentages of SWCNTs (Fig. 10). The addition of SWCNTs caused the exotherm peak of pure Azo-COOH-Py BZ to shift to lower temperature. For example, the temperature of the exotherm peak for Azo-COOH-Py BZ shifted from 226 °C to 215, 194, 193, 192, and 190 °C after blending with 0.5, 1, 2, 3, and 4 wt% of SWCNTs, respectively, and then increased slightly to

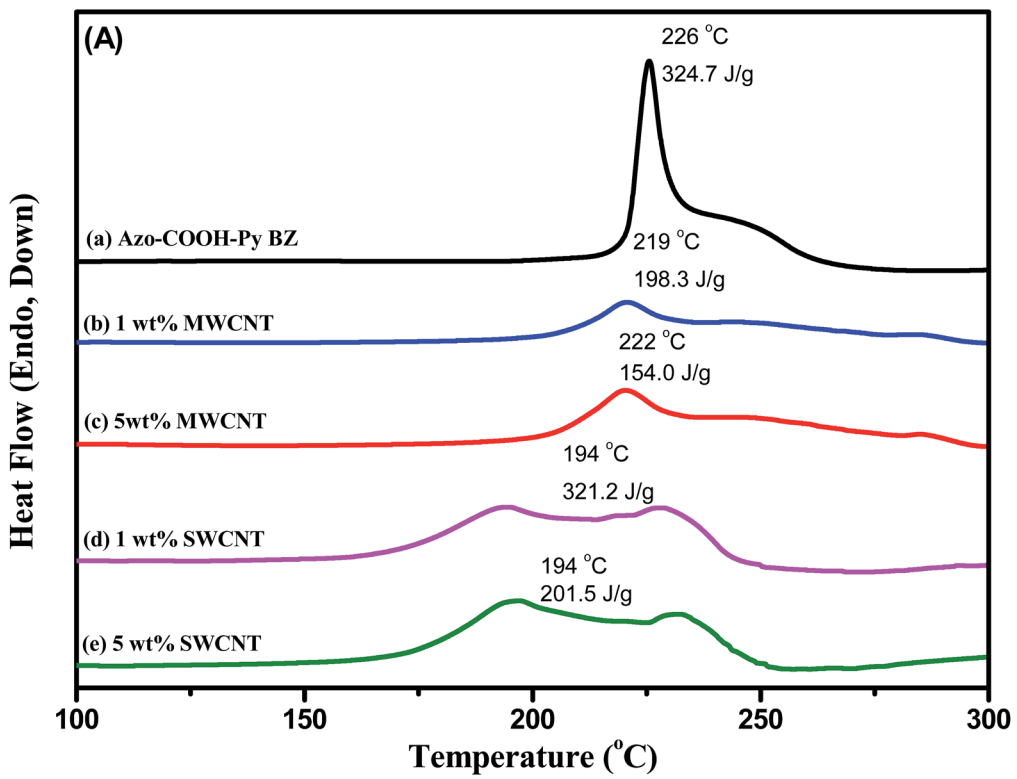

Fig. 12 DSC thermograms of the curing behavior of (a) Azo-COOH-Py BZ and (b–e) its nanocomposites with (b) 1 wt% MWCNTs, (c) 5 wt% MWCNTs, (d) 1 wt% SWCNTs, and (e) 5 wt% SWCNTs.

194 °C at 5 wt% of SWCNTs. The maximum decrease in the curing temperature was approximately 36 °C (4 wt% SWCNTs) when compared with that of the pure Azo-COOH-Py BZ monomer and approximately 96 °C when compared with that of the Py-BZ monomer, implying increasingly rapid thermal curing of the BZ monomers. Previous studies have confirmed that CNTs can act as catalysts for polymer resins and initiate early state curing.[3,45,46] Thus, we attribute the decrease in the curing temperatures to the catalytic effect of the SWCNTs on the opening of the BZ ring, thereby accelerating the curing process at lower temperatures. Our results suggest that both the COOH unit on the aromatic ring and the SWCNTs led to acceleration of the curing process at lower temperature. As mentioned above, Chen *et al.* reported that the surface COOH groups of CNTs catalyzed and decreased the curing temperature of the BZ monomer;[22] such covalent functionalization of CNTs would, however, worsen their optical, electronic, and mechanical properties. Our approach described herein has two advantages: (i) the Azo-COOH-Py BZ monomers facilitated dispersion of the CNTs through π–π stacking between the pyrene units and the CNTs; (ii) it does not lower the number of sp^2-hybridized carbon atoms in the CNTs (as does covalent functionalization with COOH groups) because the COOH groups of the Azo-COOH-Py BZ monomers acted as catalysts for thermal curing. In addition, the total exotherm for the Azo-COOH-Py BZ/SWCNT nanocomposites decreased from 324.7 J g^{-1} (for pure Azo-COOH-Py BZ) to 201.5 J g^{-1} at 5 wt% SWCNT content, indicating that blending with SWCNTs hindered the mobility of the ring-opened BZ, thereby decreasing the crosslinking density of the PBZ.[46]

We also studied the curing behavior of the Azo-COOH-Py BZ/SWCNT (5 wt%) hybrid complex after each curing stage as shown in Fig. 11. The enthalpy of the exotherm of the mixture gradually decreased upon increasing the temperature of the curing process, finally reaching zero when the curing temperature was 240 °C. The result is similar to the curing behavior of pure Azo-COOH-Py BZ [Fig. 4(A)], where first exotherm disappeared at 180 °C, but the first exotherm peak temperature after adding 5 wt% SWCNTs increased upon increasing the curing temperature. Therefore, SWCNTs have a catalytic effect on the ring opening reactions of BZ monomers, but they also hinder the mobility of the PBZ polymers after thermal curing.

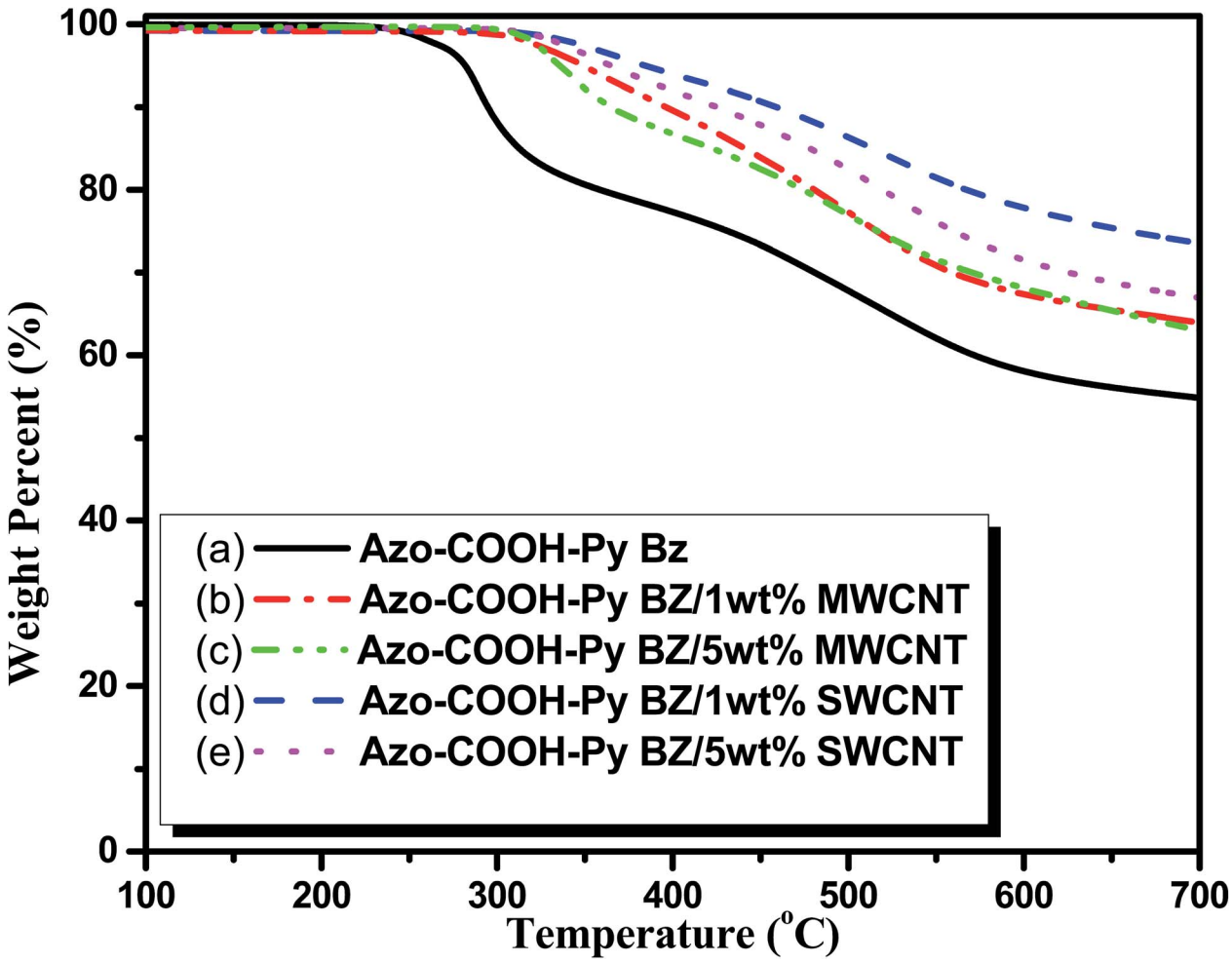

Fig. 13 TGA analyses of (a) Azo-COOH-Py BZ and (b–e) its nanocomposites with (b) 1 wt% MWCNTs, (c) 5 wt% MWCNTs, (d) 1 wt% SWCNTs, and (e) 5 wt% SWCNTs after thermal curing.

We observed similar curing behavior during DSC analysis of the Azo-COOH-Py BZ/MWCNT (5 wt%) nanocomposite (Fig. S2†).

We also examined the curing behavior of the Azo-COOH-Py BZ monomer after blending with SWCNTs or MWCNTs at the same weight percentages (Fig. 12). The maximum exothermic temperatures and the enthalpies of the curing exotherm decreased significantly upon increasing the content of MWCNTs or SWCNTs. More interestingly, the SWCNTs lowered the curing temperature, but increased the enthalpy of the exotherm, indicating that they acted as stronger catalysts and provided a higher crosslinking density than did the MWCNTs for the ring opening of the BZ monomer in this study. This result was probably due to the better thermal conductivity of the SWCNTs enhancing the thermal curing behavior of the BZ ring.[47]

Fig. 13 presents the thermal stabilities under N_2 of pure Azo-COOH-Py BZ and its blends with SWCNTs and MWCNTs after thermal curing at 210 °C, to eliminate the effect of decarboxylation, as investigated using TGA. The addition of MWCNTs or SWCNTs increased both the thermal decomposition temperature and the char yield of Azo-COOH-Py BZ, because the incorporated CNTs blocked the premature evaporation of decomposed molecular fragments and led to the formation of network structures for the nanohybrids.[45,46] Nevertheless, the thermal decomposition temperature and char yield in the presence of 1 wt% MWCNTs or SWCNTs were better than those in the presence of 5 wt% MWCNTs or SWCNTs. We attribute the lower thermal decomposition temperatures to the lower crosslinking densities after blending with 5 wt% MWCNTs or SWCNTs, because the amount of the exotherm in the presence of 5 wt% MWCNTs or SWCNTs was lower than that in the presence of 1 wt% MWCNTs or SWCNT; alternatively, some aggregation of CNTs may have occurred at relatively high CNT loadings. The thermal decomposition temperature and char yield in the presence of SWCNTs were greater than those in the presence of MWCNTs, probably because of the greater thermal conductivity of the SWCNTs enhanced the crosslinking density of the PBZ matrix. Finally, a conventional typical 3-phenyl-3,4-dihydro-2*H*-benzooxazine (Pa-type, without azobenzene, COOH, or pyrene groups) exhibits its thermal curing peak at 263 °C and a char yield of approximately 45 wt% after thermal curing.[3] In this study, our Azo-COOH-Py BZ monomer in the presence of only 1 wt% SWCNTs exhibited a much lower thermal curing temperature (194 °C) but a significantly higher char yield (*ca.* 74 wt%) after thermal curing, suggesting potential applications in nitrogen-doped carbon-based materials.

Conclusion

We have prepared a new multifunctional Azo-COOH-Py BZ monomer, containing azobenzene, COOH, and pyrene units, that enhances the solubility of CNTs in THF, leading to highly dispersible Azo-COOH-Py BZ/CNT organic/inorganic hybrid matrixes. The thermal curing temperature of Azo-COOH-Py BZ was much lower than that of the traditional pyrene-based BZ monomer, because the azobenzene and COOH units served as catalysts for the thermal curing process. We also found that after blending Azo-COOH-Py BZ with CNTs, the exothermic curing peak decreased from 226 to 190 °C (SWCNTs), confirming that incorporation of the CNTs into the PBZ matrix catalyzed the thermal curing process. The thermal decomposition temperature and char yield increased significantly, however, after addition of the CNTs into poly(Azo-COOH-Py BZ) because of both the crosslinked structure and the presence of the inorganic CNTs. In addition, the thermal decomposition temperature and char yield in the presence of the SWCNTs were better than those in the presence of the MWCNTs, presumably because the greater thermal conductivity of the SWCNTs enhanced the crosslinking density of the PBZ matrix. This combination of multifunctional units on the BZ structure significantly decreased the curing temperature, but provided a polymeric matrix exhibiting significantly greater thermal stability.

Acknowledgements

This study was financially supported by the Ministry of Science and Technology, Taiwan under contracts MOST103-2221-E-110-079-MY3 and MOST102-2221-E-110-008-MY3. We also thank Mr Hsien-Tsan Lin of the Regional Instruments Center at National Sun Yat-Sen University for help with the TEM measurement. In addition, Prof. Dai would like to thank the National Natural Science Foundation of China (U1205113).

References

1 C. P. R. Nair, *Prog. Polym. Sci.*, 2004, **29**, 401–498.
2 N. N. Ghosh, B. Kiskan and Y. Yagci, *Prog. Polym. Sci.*, 2007, **32**, 1344–1391.
3 H. Ishida, *Handbook of Polybenzoxazine Resins*, ed. H. Ishida and T. Agag, Elsevier, Amsterdam2011, ch. 1, p. 1.
4 C. F. Wang, Y. C. Su, S. W. Kuo, C. F. Wang, Y. C. Sheen and F. C. Chang, *Angew. Chem., Int. Ed.*, 2006, **45**, 2248–2251.
5 A. Sudo, R. Kudo, H. Nakayama, K. Arima and T. Endo, *Macromolecules*, 2008, **41**, 9030–9034.
6 C. F. Wang, F. C. Chang, and S. W. Kuo, *Handbook of Polybenzoxazine*, ed. H. Ishida and T. Agag, Elsevier, Amsterdam2011, ch. 33, p. 579.
7 Y. Yagci, B. Kiskan and N. N. Ghosh, *J. Polym. Sci., Part A: Polym. Chem.*, 2009, **47**, 5565–5576.
8 Q. Li and X. Zhong, *Langmuir*, 2007, **27**, 8365–8369.
9 M. R. Vengatesan, S. Devaraiu, K. Dinkaran and M. Alagar, *J. Mater. Chem.*, 2012, **22**, 7559–7566.
10 S. W. Kuo, Y. C. Wu, F. C. Wang and K. U. Jeong, *J. Phys. Chem. C*, 2009, **113**, 20666–20673.
11 G. Ligadas, A. Tuzun, J. C. Ronda, M. Galia and V. Cadiz, *Polym. Chem.*, 2014, **5**, 636–6644.
12 C. F. Wang, S. F. Chiou, F. H. Ko, J. K. Chen, C. T. Chou, C. T. Huang, S. W. Kuo and F. C. Chang, *Langmuir*, 2007, **23**, 5868–5871.
13 S. C. Lin, C. S. Wu, J. M. Yeh and Y. L. Liu, *Polym. Chem.*, 2014, **5**, 4235–4244.
14 C. H. Lin, S. L. Chang, T. Y. Shen, Y. S. Shih, H. T. Lin and C. F. Wang, *Polym. Chem.*, 2012, **3**, 935–945.

15 H. Ishida and H. Y. Low, *J. Appl. Polym. Sci.*, 1998, **69**, 2559–2567.
16 J. Jang and H. Yang, *J. Mater. Sci.*, 2000, **35**, 2297–2303.
17 S. W. Kuo and F. C. Chang, *Prog. Polym. Sci.*, 2011, **36**, 1649–1696.
18 M. C. Tseng and Y. L. Liu, *Polymer*, 2010, **51**, 5567–5575.
19 K. W. Huang and S. W. Kuo, *Macromol. Chem. Phys.*, 2010, **211**, 2301–2311.
20 Y. C. Wu and S. W. Kuo, *Polymer*, 2010, **51**, 3948–3955.
21 C. R. Arza, H. Ishida and F. H. J. Maurer, *Macromolecules*, 2014, **47**, 3685–3692.
22 Q. Chen, R. Xu and D. Yu, *Polymer*, 2006, **47**, 7711–7719.
23 N. G. Sahoo, S. Rana, J. W. Cho, L. Li and S. H. Chan, *Prog. Polym. Sci.*, 2010, **35**, 837–867.
24 Y. P. Sun, K. F. Fu, Y. Lin and W. J. Huang, *Acc. Chem. Res.*, 2002, **35**, 1096–1104.
25 J. M. Huang, M. F. Tsai, S. J. Yang and W. M. Chiu, *J. Appl. Polym. Sci.*, 2011, **122**, 1898–1904.
26 C. F. Wang, S. W. Kuo, C. H. Lin, H. G. Chen, C. S. Liao and P. R. Hung, *RSC Adv.*, 2014, **4**, 36012–36016.
27 L. Dumas, L. Bonnaud, M. Olivier and P. Dubois, *Chem. Commun.*, 2013, **49**, 9543.
28 C. C. Yang, Y. C. Lin, P. I. Wang, D. J. Liaw and S. W. Kuo, *Polymer*, 2014, **55**, 2044–2050.
29 M. G. Mohamed, K. C. Hus and S. W. Kuo, *Polym. Chem.*, 2015, **6**, 2423–2433.
30 C. Zuniga, L. Bonnaud, G. Ligadas, J. C. Ronda, M. Galia, V. Cadiz and P. Dubois, *J. Mater. Chem. A*, 2014, **2**, 6814–6822.
31 S. Iijima, *Nature*, 1991, **354**, 56–58.
32 E. Thostenson, Z. Ren and T. W. Chou, *Compos. Sci. Technol.*, 2001, **61**, 1899–1912.
33 P. C. Ma, N. A. Siddiqui, G. Marom and J. K. Kim, *Composites, Part A*, 2010, **41**, 1345–1367.
34 D. Tasis, N. Tagmatarchis, A. Biano and M. Prato, *Chem. Rev.*, 2006, **106**, 1105–1136.
35 M. G. Mohamed, C. H. Hsiao, K. C. Hsu, F. H. Lu, H. K. Shih and S. W. Kuo, *RSC Adv.*, 2015, **5**, 12763–12772.
36 T. Asano, T. Yano and T. Okada, *J. Am. Chem. Soc.*, 2002, **124**, 8398–8405.
37 H. Lee, J. Pietrasik and K. Matyiaszewski, *Macromolecules*, 2006, **39**, 3914–3920.
38 C. J. Barrett, J. Mamiaya, G. K. Yagar and T. Ikeda, *Soft Mater.*, 2007, **3**, 1249–1261.
39 B. Kiskan and Y. Yagci, *Polymer*, 2005, **46**, 11690–11697.
40 R. Andreu, J. A. Reina and J. C. Ronda, *J. Polym. Sci., Part A: Polym. Chem.*, 2008, **46**, 6091–6101.
41 A. Natansohn and P. Rochon, *Chem. Rev.*, 2002, **102**, 4139–4175.
42 G. S. Kumar and D. C. Neckers, *Chem. Rev.*, 1989, **89**, 1915–1925.
43 W. Jiang, G. Wang, Y. He, X. Wang, Y. An, Y. Song and L. Jiang, *Chem. Commun.*, 2005, 3550–3552.
44 H. Murakami, T. Nomura and N. Nakashima, *Chem. Phys. Lett.*, 2003, **378**, 481–485.
45 M. Chapartegui, J. Barcena, X. Irastorza, C. Elizetxea, M. Fernandez and A. Santamaria, *Compos. Sci. Technol.*, 2012, **72**, 489–497.
46 M. Kaleemullah, S. W. Khan and J. K. Kim, *Compos. Sci. Technol.*, 2012, **72**, 1968–1976.
47 J. Che, T. Cagin and W. A. Goddard III, *Nanotechnology*, 2000, **11**, 65.